The inversion framework: Our inversion framework is built upon the TM5 4DVar system (Meirink et al., 2008), modified to jointly assimilate measurements of CO_2 and $\Delta^{14}CO_2$ in a multi-tracer inversion framework (Basu et al., 2020; Basu et al., 2016). The isotopic mass balance equations for this framework can be found in Basu et al. (2016). In the main text we describe the cost function to be minimized in order to estimate five fluxes categories (Section 2.3). We followed the prescription of Basu et al. (2016) to set up the prior covariance (B) for the five flux categories, keeping the default "hybrid" prior correlation structure unchanged but changing the prior uncertainties (σ in Table 1 of Basu et al. (2016)). Table S2 lists prior uncertainties for both years along with previously assigned uncertainties for the five flux categories. Posterior flux sensitivity to alternate specifications of temporal and spatial error correlations (C_t and C_r respectively in eq. 4 of Basu et al. (2016)) are discussed in the main text. For $\Delta^{14}CO_2$ observations, we constructed elements of R as the quadrature sum of a measurement uncertainty of 1.8‰ and a transport model error computed from modeled tracer gradients across neighboring cells. For CO_2 observations, the elements of *R* were quantified following the empirical scheme used in the CarbonTracker 2022 data assimilation system (Jacobson et al., 2023). This differs from our previous studies (Basu et al., 2020; Basu et al., 2016) in which elements of *R* for CO_2 measurements were calculated as the quadrature sum of a model uncertainty (computed as above) and a site-specific measurement uncertainty.

Initial concentrations:
Our inversion setup for year Y optimizes fluxes for six months (July—December) in year Y-1, and three months (January—March) in year Y+1, following earlier work (Basu et al., 2020; Basu et al., 2016). The two largest contributions to the uncertainty of the initial $\Delta^{14}CO_2$ field on July 1 of either 2009 or 2014 are (a) the vertical profile of $\Delta^{14}CO_2$ that is a balance between ^{14}C production in the upper atmosphere and the oceanic $^{14}CO_2$ sink, and (b) a possible offset in the initial $\Delta^{14}CO_2$ field due to the insufficiency of background measurements to constrain it. To test the sufficiency of our spin-up period and the impact of the above uncertainties on derived $FFCO_2$ estimates, we performed two sets of experiments for Basu et al. (2016) and Basu et al. (2020). First, we performed three inversions with three different initial $\Delta^{14}CO_2$ fields derived from the three possible stratospheric $^{14}CO_2$ injection profiles discussed in Miller et al. (2025). Second, we performed an alternate inversion by adding a 3‰ uniform offset to the initial $\Delta^{14}CO_2$ field. In both those experiments, the derived $FFCO_2$ fluxes after three months, i.e., after September 2009, were virtually indistinguishable across the different inversions. This led us to conclude that a six-month spin-up was sufficient for constraining FF CO_2 fluxes in our setup. We also desired a spin-down period of sufficient length using measurements in either 2011 or 2016 to accurately constrain end of year fluxes in 2010/2015. In the northern temperate latitudes, air typically circumnavigates the globe in 2-3 weeks, and the air mass north of 25°N – where the majority of our $\Delta^{14}CO_2$ measurements are located becomes well-mixed within ~3 months. Hence, we specify a three-month spin-down period.

The initial fields of CO_2 and $CO_2 \times \Delta^{14}CO_2$ on July 1, 2009 and 2014, needed for the two inversion years 2010 and 2015 respectively, were constructed slightly differently. We ran a forward simulation of the two tracers from Jan 1, 2000 to Jan 1, 2008 using the fluxes detailed in Miller et al. (2025). We then performed a multi-tracer CO_2 and $\Delta^{14}CO_2$ inversion from Jan 1, 2008 to

Jul 1, 2009, and used the posterior fields on that ending date as the initial fields for our year 2010 inversion. To obtain the initial fields on Jul 1, 2014 for our year 2015 inversion, we scaled the posterior mole fraction fields on Apr 1, 2011 that resulted from our year 2010 inversion. Specifically, to scale the 3D $CO_2 \times \Delta^{14}CO_2$ field, we first obtained the global average $\Delta^{14}CO_2$ for 01 April 2011 and 01 July 2014 from the long-term Northern and Southern hemispheric records. We multiplied these two values by the corresponding global mean marine surface CO_2 concentrations, and then subtracted the 01 July 2014 quantity from the 01 April 2011 quantity. The resulting difference of approximately 5 was uniformly subtracted from the posterior 3D $CO_2 \times \Delta^{14}CO_2$ field of 01 April 2011 to yield the scaled 3D field for 01 July 2014. The scaled 3D CO_2 field was obtained more simply by uniformly multiplying the 3D CO_2 field of 01 April 2011 by the ratio of the global mean marine surface CO_2 concentration between 01 July 2014 and 01 April 2011. Given the results showing insensitivity to deliberate misrepresentation of initial fields after 3 months of spin-up, sensitivity to small errors in our specified estimates of initial $CO_2 \times \Delta^{14}CO_2$ fields in either year is expected to be negligible.

Table S1: $\Delta^{14}CO_2$ observing sites and relevant measurement laboratories along with the number of site specific assimilated $\Delta^{14}CO_2$ observations for each inversion period and those for Basu et al. (2020).

Site Name	Code	Lat/Lon	Group	Platform	Assimilated Observations (n)[a]		
					2010 (Basu et al., 2020)	2010-update	2015
Alert, NU, Canada	ALT	82.5/-62.31	Environment and Climate Change Canada	Surface	0	16	33
Argyle, ME, USA	AMT	45.03/-68.68	NOAA	Surface	101	101	133
Barrow, AK, USA	BRW	71.32/-156.61	NOAA	Surface	89	89	78
Cape Grim, TAS, AU	CGO	-40.68/144.69	SIO	Surface	22	32	23
Offshore Cape May, NJ, USA	CMA	38.78/-74.56	NOAA	Aircraft	130	119	83
Carbon in Arctic Reservoirs Vulnerability Experiment (CARVE), AK, USA	CRV	60.41/-164.04	NOAA	Aircraft	0	0	3
Dahlen, ND, USA	DND	47.24/-99.49	NOAA	Aircraft	0	0	51
Drake Passage	DRP	-59.18/-65.42	NOAA	Shipboard	42	21	29
Estevan Point, BC, CAN	ESP	49.34/-126.56	NOAA	Aircraft	0	0	65
Harvard Forest, MA, USA	HFM	42.54/-72.17	Harvard University	Surface	0	0	6
Indianapolis flux Experiment (INFLUX), IN, USA[b]	INX	39.58/-86.52	NOAA	Surface	16	16	88
Izana, Tenerife, Canary Islands, ESP	IZO	28.31/-16.5	AEMET	Surface	0	37	37
Jungfraujoch, CH	JFJ	46.55/7.99	KUP	Surface	21	1	45
Park Falls, WI, USA	LEF	45.78/-90.37	NOAA	Surface and Aircraft	150	150	194

Mt. Bachelor Observatory OR, USA	MBO	43.98/-121.69	NOAA	Surface	0	0	45
Mace Head, County Galway, Ireland	MHW	53.33/-9.9	NOAA	Surface	0	6	43
Mt. Wilson Observatory CA, USA	MWO	34.22/-118.06	NOAA	Surface	58	57	73
Offshore Portsmouth, NH, USA	NHA	42.82/-70.63	NOAA	Aircraft	92	89	79
Niwot Ridge, CO, USA	NWR	40.05/-105.59	NOAA	Surface	133	68	75
Pacific Ocean	POC	-30.82/-178.72	NOAA	Shipboard	0	0	179
Beech Island, SC, USA	SCT	33.41/-81.83	NOAA	Surface	167	166	178
Schauinsland, Baden-Wuerttemberg DE	SSL	47.9/7.92	SCHAU	Surface	20	0	0
Tae-ahn Peninsula, KOR	TAP	36.73/126.13	NOAA	Surface	46	0	0
West Branch, IA, USA	WBI	41.72/-91.35	NOAA	Surface	0	0	146
Walnut Grove, CA, USA	WGC	38.26/-121.49	NOAA	Surface	238	237	179
Moody, TX, USA	WKT	31.31/-97.33	NOAA	Surface	179	174	170
Total					1,504	1,379	2,035

[a]Values refer to total number of observations assimilated in each 21-month inversion period, which includes bounding months of adjacent years (6 months before and 3 months after).
[b]INX data are from (Turnbull et al., 2015) and (Turnbull et al., 2019), assimilating only measurements from towers upwind of the Indianapolis urban area.

Table S2: Assigned prior uncertainties for the five optimized fluxes aggregated globally (for land or ocean) and for the U.S. for three experimental set-ups. Prior uncertainties for 2010 and 2015 differ because they scale to prior fluxes or prior flux components which differ from year to year. Here F_{bio} is equivalent to NBE. Absolute U.S. and global flux totals are given in **Table S6**.

Flux	**Experimental set-up**					
	2010 (*Basu et al. (2020)*)		**2010 (this study)**		**2015 (this study)**	
	Global	**U.S.**	**Global**	**U.S.**	**Global**	**U.S.**
F_{fos} (TgC/yr)	*340*	*120*	693	119	807	117
F_{bio} (TgC/yr)	*1344*	*313*	1344	313	1306	317
F_{oce} (TgC/yr)	*699*	--	699	--	734	--
F_{biodis} (PgC ‰/yr)	*519*	*84*	1021	165	1110	176
F_{ocedis} (PgC ‰/yr)	*819*	--	792	--	793	--

Table S3: Impact of updated U. of Heidelberg CORSO data on annual national total posterior $FFCO_2$ and NBE for 2010 using the Miller/CT2022 $FFCO_2$ and CT2016 NBE priors. CORSO site codes and numbers of observations are given in **Table S4**.

Experiment	**U.S. FFCO2 (TgC/yr)**	**U.S. NBE (TgC/Yr)**	**U.S. Total Carbon (TgC/yr)**
w/o update	1745	-231	1514
w/ update	1755	-240	1515
Difference	**10**	**9**	**1**

Table S4: CORSO site codes with numbers of assimilated ^{14}C observations for 2010 with and without the CORSO data update. Site names and locations are given in **Table S1**.

Site code	No. of obs. with update	No. of obs. w/o update
ALT	21	12
CGO	19	19
IZO	19	19
JFJ	18	0
MHW	22	2
MQA	18	0
NMY	23	0
Total	**140**	**52**

Table S5: Adjustment categories and their national totals along with reported and adjusted national and regional $FFCO_2$ totals for EPA (EPA, 2024) and Vulcan 3.0 (Gurney et al., 2020a; Gurney et al., 2020b) reported emissions. Regional adjustments are assumed to scale to the regional fraction of total $FFCO_2$ emission for either EPA or Vulcan. The basis for imposed adjustments is discussed in Basu et al. (2020).

		2010 (TgC/yr)	**2015 (TgC/yr)**
Adjustment category and national total	U.S. Bio Fuel [*BF*][a]	20.1	24.6
	U.S. Domestic aviation [*DA*][b]	41.8	43.4
	U.S. International aviation [*IA*][c]	37.0	37.0
	All in-country aviation up to 3000 ft [*DA3000*][c]	20.0	20.0
EPA reported national and regional totals	U.S. National [EPA_{NR}]	1537.6	1456.7
	U.S. West [EPA_{WR}]	270.4	263.5
	U.S. Center [EPA_{CR}]	423.8	423.6
	U.S. East [EPA_{ER}]	843.5	769.5
EPA adjusted national and regional totals	U.S. National [$EPA_{NA} = EPA_{NR} + IA$]	1574.6	1493.7
	U.S. West [$EPA_{WA} = EPA_{WR} \times EPA_{NA} / EPA_{NR}$]	276.9	270.2
	U.S. Center [$EPA_{CA} = EPA_{CR} \times EPA_{NA} / EPA_{NR}$]	434.0	434.4
	U.S. East [$EPA_{EA} = EPA_{ER} \times EPA_{NA} / EPA_{NR}$]	863.8	789.1
Vulcan reported national and regional totals	U.S. National [V_{NR}]	1638.9	1544.0
	U.S. West [V_{WR}]	303.6	297
	U.S. Center [V_{CR}]	400.2	388
	U.S. East [V_{ER}]	935	858.9
Vulcan adjusted national and regional totals	U.S. National [$V_{NA} = V_{NR} + DA + IA - DA3000 - BF$]	1677.6	1579.8
	U.S. West [$V_{WA} = V_{WR} \times V_{NA} / V_{NR}$]	310.8	303.9
	U.S. Center [$V_{CA} = V_{CR} \times V_{NA} / V_{NR}$]	409.6	397.0
	U.S. East [$V_{EA} = V_{ER} \times V_{NA} / V_{NR}$]	957.1	878.8

[a]EIA (2024)

[b]Table 2-13, excel file, in the Inventory of U.S. Greenhouse gas emissions and Sinks: 1990-2022 (EPA, 2024),

[c]see Basu et al. (2020)

Table S6: Annual U.S. and global totals for prior fluxes used in the analysis. F_{biodis} and F_{ocedis} refer to the isotopic fluxes associated with terrestrial biological disequilibrium and ocean disequilibrium.

Flux types	name	2010		2015	
		U.S.	Global	U.S.	Global
$FFCO_2$ (TgC/yr)	Miller/CT	1532	8993	1465	9627
	FFDAS	1485	8267	1433	8891
	ODIAC	1552	9001	1496	9633
NBE (TgC/yr)	CT16	-283	-1334	-111	-266
	CT19B	-343	-971	-263	-794
	SiB4	-211	-1949	-201	-1804
Net Ocean (TgC/yr)	CT16	N/A	-2978	N/A	-3350
	CT19B	N/A	-2919	N/A	-3144
	SiB4	N/A	-2919	N/A	-3144
Isotopic (PgC‰/yr)	F_{biodis}	183	2446	196	2632
	F_{ocedis}	N/A	-1504	N/A	-683
	Nuclear	100	486	100	486
	Cosmogenic	N/A	466	N/A	3883

Table S7: 9-member uncertainty-weighted posterior mean and prior mean fluxes for 2010 and 2015, along with related MC-based uncertainties (1σ) and the standard deviation (1σ) of the ensemble-wide spread. Note that prior uncertainties for the SiB4-based NBE priors differ from those for the two NBE priors, leading to different posterior uncertainties for experiments using the SiB4 prior (see **Section 2.4**). MC-based uncertainties for these experiments are shown as subjacent bracketed values.

Prior or posterior by year	Flux (9-member mean) TgC/yr			Uncertainty [using SiB4] TgC/yr			9-member Ensemble S.D. (1σ) TgC/yr		
	Total Carbon	Fossil	NBE	Total Carbon	Fossil	NBE	Total Carbon	Fossil	NBE
2010-prior	1227	1523	-298	196 [310]	78 [77]	174 [302]	64	30	57
2010-post	1434	1715	-282	33 [79]	26 [49]	41 [94]	106	45	135
2015-prior	1276	1465	-189	184 [315]	69 [73]	163 [307]	72	27	66
2015-post	1631	1578	54	32 [57]	29 [37]	37 [64]	107	59	130

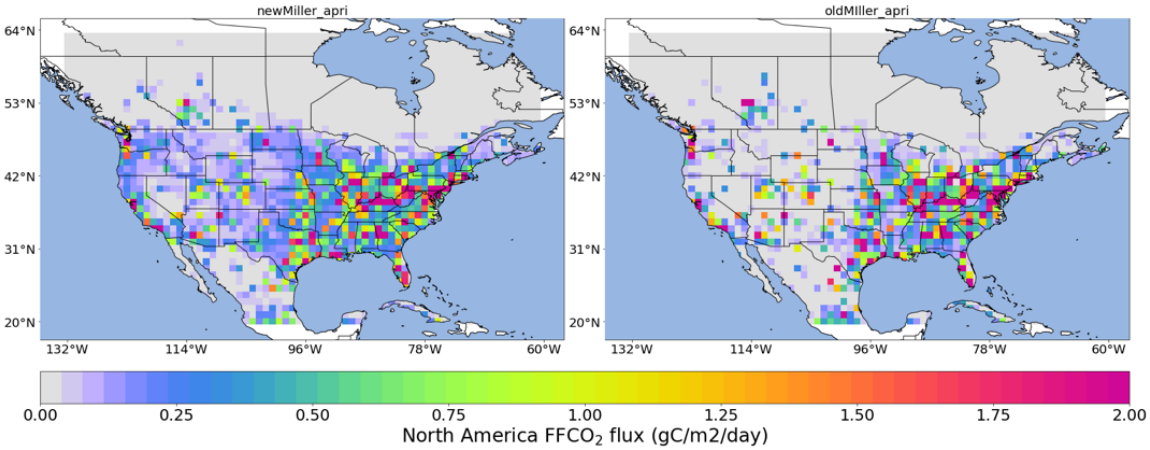

Figure S1: Annual mean $FFCO_2$ for 2010 for the updated Miller/CT2022 flux prior (left) compared to that from the Miller/CT2016 $FFCO_2$ prior used in Basu et al. (2020), both gridded at the zoom region resolution of 1°x1°. Note the significant change in prior emissions in the western half of the country discussed in the main text.

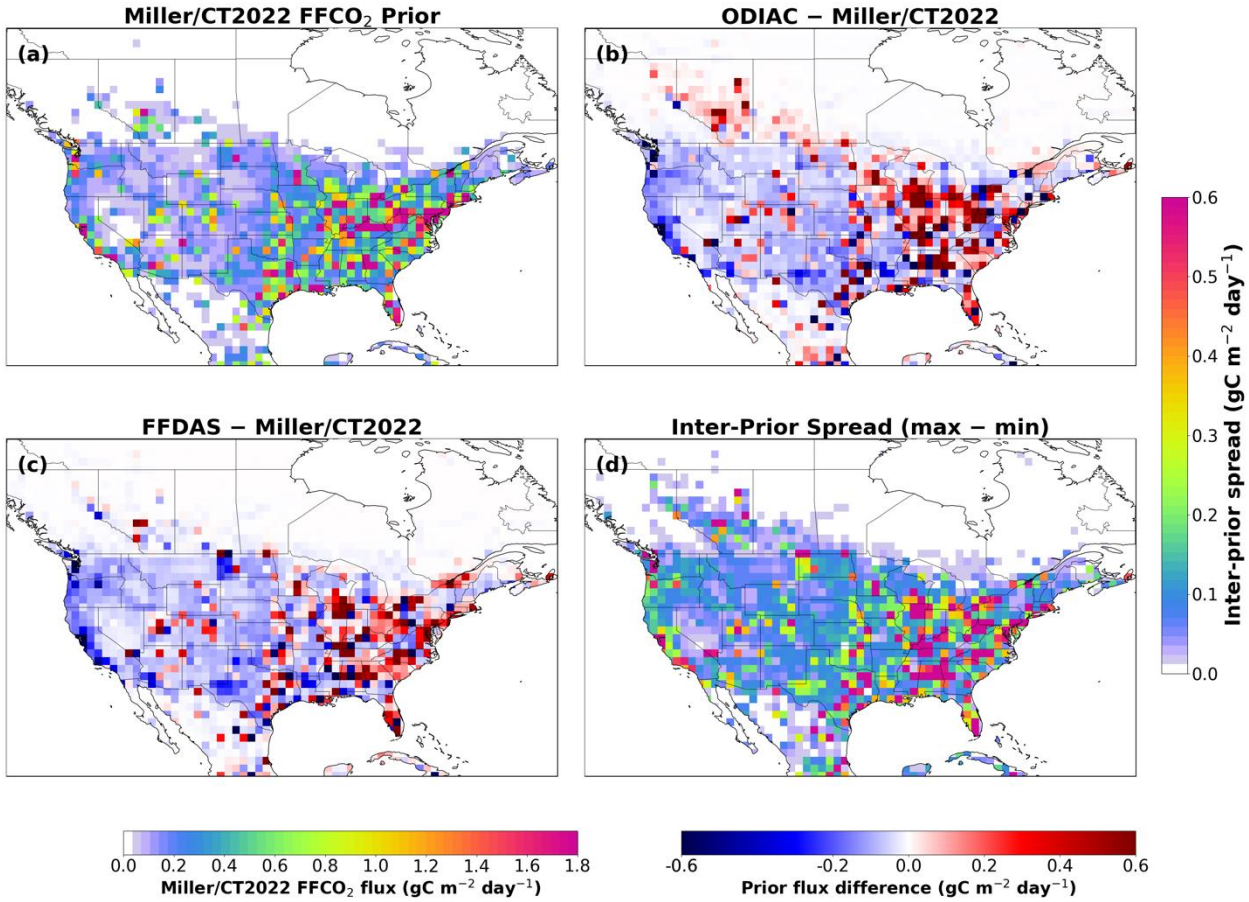

Figure S2. a) Annual mean Miller/CT2022 $FFCO_2$ flux prior for 2015 gridded at the zoom region resolution of 1°x1°; b) the difference between the annual average $FFCO_2$ prior from ODIAC and from Miller/CT2022 for 2015; c) same as b) but for the difference between FFDAS and Miller/CT2022; d) the inter-prior spread (maximum to minimum) across all three priors, which is used to estimate prior $FFCO_2$ uncertainty as discussed in the main text.

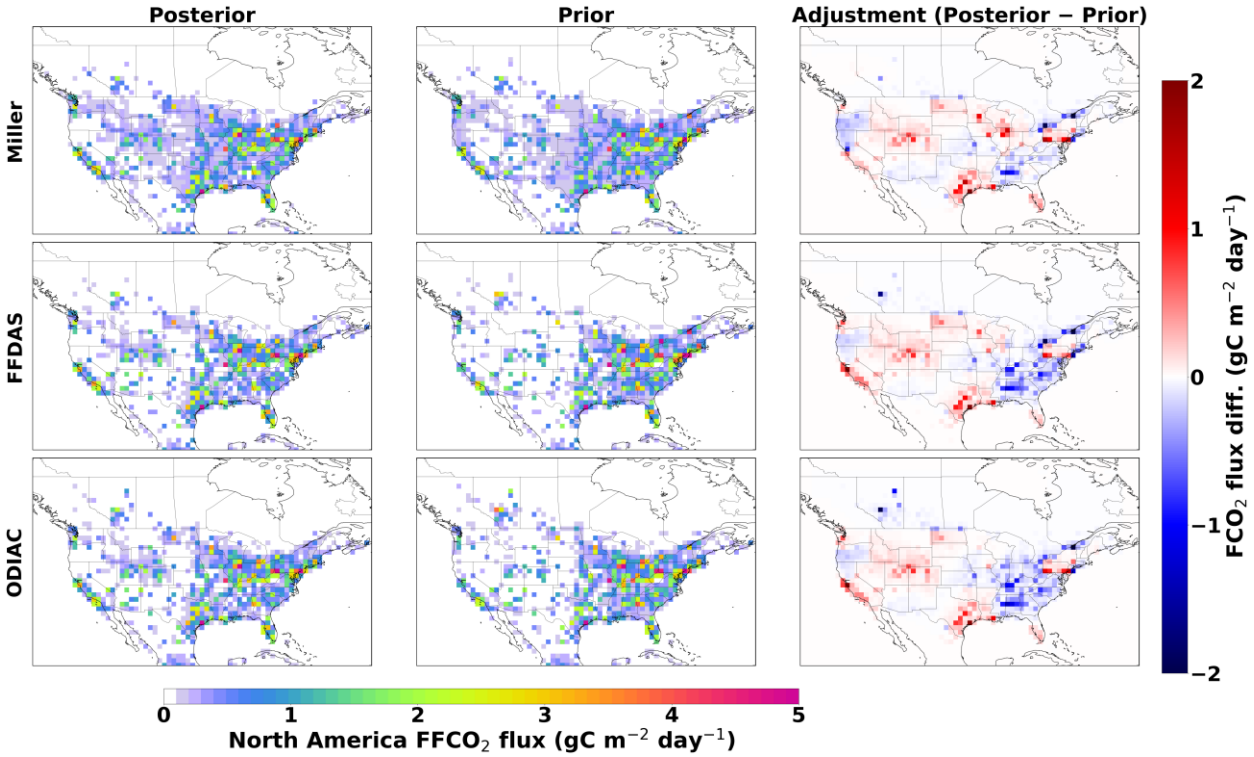

Figure S3: Spatial patterns of prior and posterior $FFCO_2$ fluxes and associated adjustments (posterior-prior differences) for 2010 for the Miller-CT2022 (top row), FFDAS (middle row), and ODIAC (bottom row) priors.

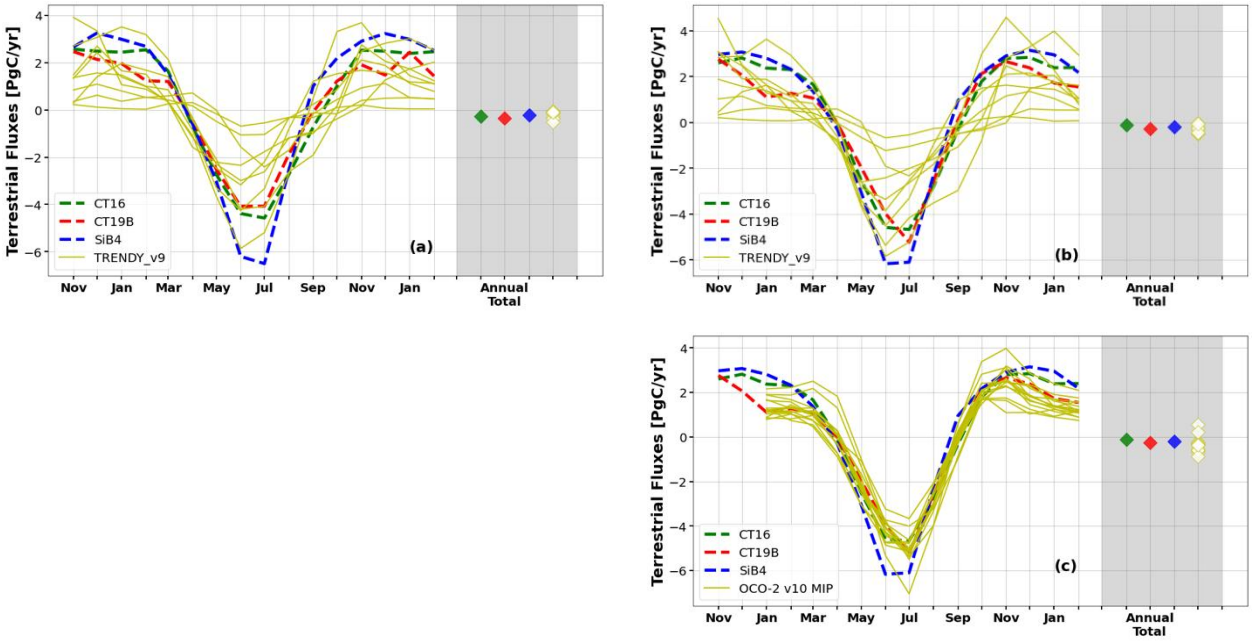

Figure S4: Representativeness of the seasonal cycle of NBE and its annual total for the three priors used here with respect to estimates from the TRENDY terrestrial biosphere model intercomparison (v9.0) (top; panels 'a' and 'b') and from the OCO-2 v10 model intercomparison (bottom; panel 'c'), for both 2010 (left, OCO-2 v10 MIP results unavailable) and 2015 (right). For OCO-2 v10 MIP, we used results for Land Nadir and Land Glint retrievals and in-situ measurements (LNLGIS) (16 models) after screening for results producing seemingly non-physical seasonal cycles, as discussed in the main text. Note that annualized NBE is given in PgC/yr, in contrast to TgC/yr used for discussion of annualized $FFCO_2$ fluxes.

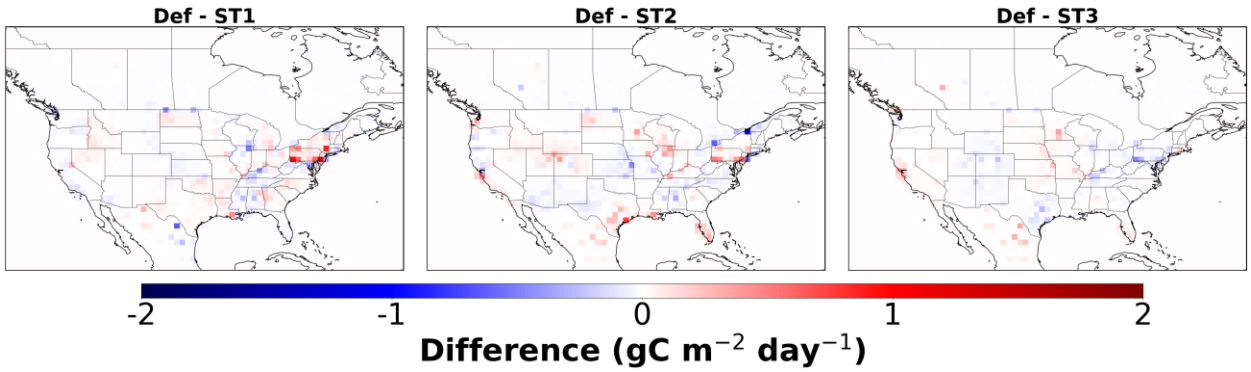

Figure S5: Impact of alternate treatments of spatiotemporal error correlations on the pattern of posterior annual $FFCO_2$ for sensitivity experiments ST1 (continuous exponential decay correlation function), ST2 (abbreviated temporal correlation length) and ST3 (increased error correlation length scale for NBE only), all vs. the default "hybrid" treatment of spatiotemporal error correlation discussed in the main text. The impact on annual national $FFCO_2$ totals are +26, +33, and 0 TgC/yr, respectively.

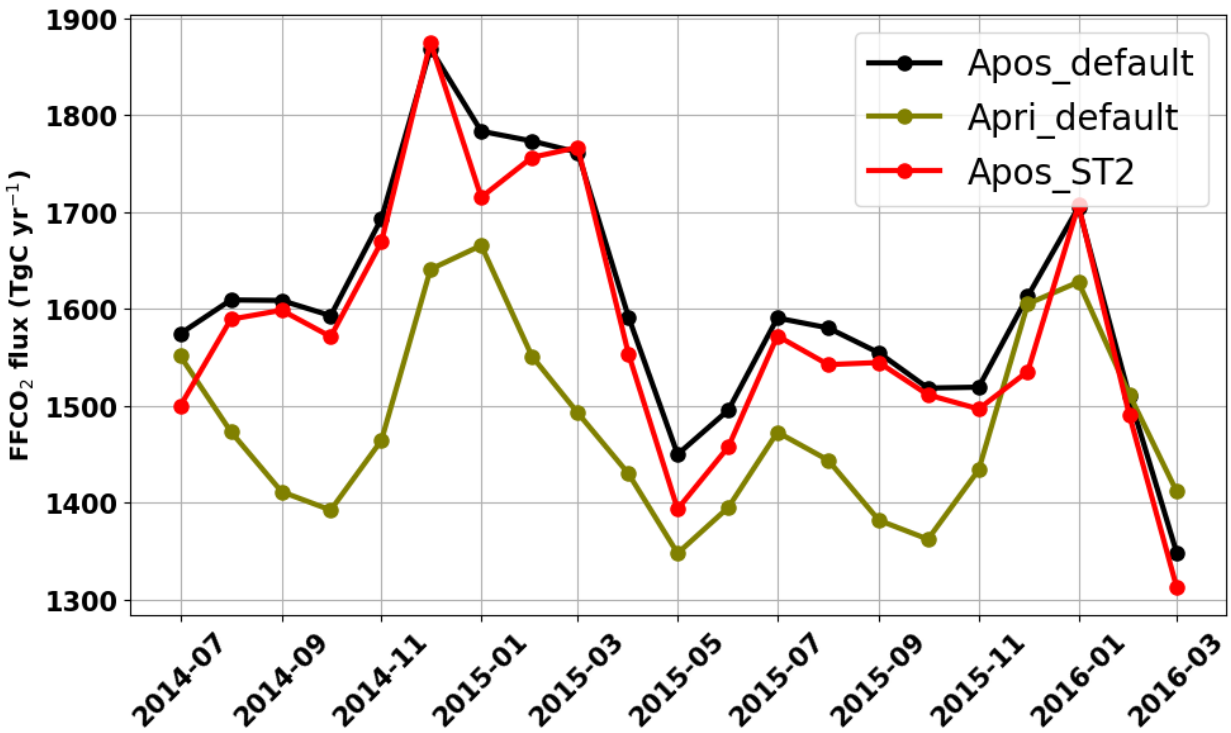

Figure S6: Monthly posterior $FFCO_2$ totals when using the abbreviated temporal correlation length scale (experiment ST2) compared to those when the default treatment discussed in the text. The associated prior $FFCO_2$ totals are given for comparison.

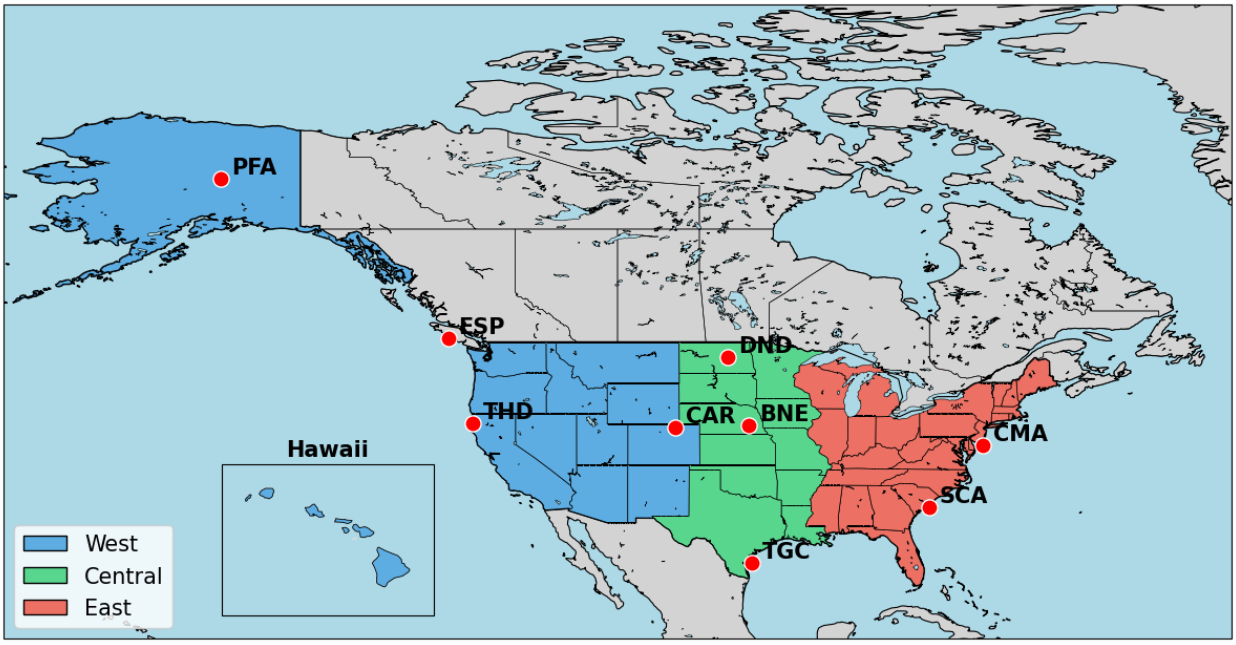

Figure S7: Locations of aircraft profiling sites in **Fig. 8**. Eastern, Central and Western U.S. regions discussed in the text are also denoted.

Supplementary References:

Basu, S., Miller, J. B., and Lehman, S.: Separation of biospheric and fossil fuel fluxes of CO_2 by atmospheric inversion of CO_2 and $^{14}CO_2$ measurements: Observation System Simulations, Atmos. Chem. Phys., 16, 5665-5683, 10.5194/acp-16-5665-2016, 2016.

Basu, S., Lehman, S. J., Miller, J. B., Andrews, A. E., Sweeney, C., Gurney, K. R., Xu, X., Southon, J., and Tans, P. P.: Estimating US fossil fuel CO_2 emissions from measurements of ^{14}C in atmospheric CO_2, Proceedings of the National Academy of Sciences, 117, 13300-13307, 10.1073/pnas.1919032117, 2020.

EIA: Monthly Energy Review: Carbon dioxide emissions from biomass energy consumption, https://www.eia.gov/totalenergy/data/monthly/pdf/sec11_10.pdf, 2024.

EPA: Inventory of U.S. Greenhouse Gas Emissions and Sinks: 1990-2022 U.S. Environmental Protection Agency, EPA 430R-24004, https://www.epa.gov/ghgemissions/inventory-us-greenhouse-gas-emissions-and-sinks-1990-2022, 2024.

Gurney, K. R., Liang, J., Patarasuk, R., Song, Y., Huang, J., and Roest, G.: Vulcan: High-Resolution Annual Fossil Fuel CO2 Emissions in USA, 2010-2015, Version 3, ORNL Distributed Active Archive Center [dataset], 10.3334/ORNLDAAC/1810, 2020a.

Gurney, K. R., Liang, J., Patarasuk, R., Song, Y., Huang, J., and Roest, G.: The Vulcan Version 3.0 High-Resolution Fossil Fuel CO2 Emissions for the United States, Journal of Geophysical Research: Atmospheres, 125, e2020JD032974, https://doi.org/10.1029/2020JD032974, 2020b.

Jacobson, A. R., Schuldt, K. N., Tans, P., Arlyn, A., Miller, J. B., Oda, T., Mund, J., Weir, B., Ott, L., Aalto, T., Abshire, J. B., Aikin, K., Aoki, S., Apadula, F., Arnold, S., Baier, B., Bartyzel, J., Beyersdorf, A., Biermann, T., Biraud, S. C., Boenisch, H., Brailsford, G., Brand, W. A., Chen, G., Huilin, C., Lukasz, C., Clark, S., Colomb, A., Commane, R., Conil, S., Couret, C., Cox, A., Cristofanelli, P., Cuevas, E., Curcoll, R., Daube, B., Davis, K. J., De Wekker, S., Coletta, J. D., Delmotte, M., DiGangi, E., DiGangi, J. P., Di Sarra, A. G., Dlugokencky, E., Elkins, J. W., Emmenegger, L., Shuangxi, F., Fischer, M. L., Forster, G., Frumau, A., Galkowski, M., Gatti, L. V., Gehrlein, T., Gerbig, C., Francois, G., Gloor, E., Gomez-Trueba, V., Goto, D., Griffis, T., Hammer, S., Hanson, C., Haszpra, L., Hatakka, J., Heimann, M., Heliasz, M., Hensen, A., Hermansen, O., Hintsa, E., Holst, J., Ivakhov, V., Jaffe, D. A., Jordan, A., Joubert, W., Karion, A., Kawa, S. R., Kazan, V., Keeling, R. F., Keronen, P., Kneuer, T., Kolari, P., Kateřina, K., Kort, E., Kozlova, E., Krummel, P., Kubistin, D., Labuschagne, C., Lam, D. H. Y., Lan, X., Langenfelds, R. L., Laurent, O., Laurila, T., Lauvaux, T., Lavric, J., Law, B. E., Lee, J., Lee, O. S. M., Lehner, I., Lehtinen, K., Leppert, R., Leskinen, A., Leuenberger, M., Levin, I., Levula, J., Lin, J., Lindauer, M., Loh, Z., Lopez, M., Luijkx, I. T., Lunder, C. R., Machida, T., Mammarella, I., Manca, G., Manning, A., Manning, A., Marek, M. V., Martin, M. Y., Matsueda, H., McKain, K., Meijer, H., Meinhardt, F., Merchant, L., Mihalopoulos, N., Miles, N. L., Miller, C. E., Mitchell, L., Mölder, M., Montzka, S., Moore, F., Moossen, H., Morgan, E., Josep-Anton, M., Morimoto, S., Müller-Williams, J., Munger, J. W., Munro, D., Myhre, C. L., Shin-Ichiro, N., Jaroslaw, N., Newman, S., Nichol, S., Niwa, Y., Obersteiner, F., O'Doherty, S., Paplawsky, B., Peischl, J., Peltola, O., Piacentino, S., Jean-Marc, P., Pickers, P., Piper, S., Pitt, J., Plass-Dülmer, C., Platt, S. M., Prinzivalli, S., Ramonet, M., Ramos, R., Reyes-Sanchez, E., Richardson, S. J., Riris, H., Rivas, P. P., Ryerson, T., Saito, K., Sargent, M., Sasakawa, M., Scheeren, B., Schuck, T., Schumacher, M., Seifert, T., Sha, M. K., Shepson, P., Shook, M., Sloop, C. D., Smith, P., Stanley, K., Steinbacher, M., Stephens, B.,

Sweeney, C., Thoning, K., Timas, H., Torn, M., Tørseth, K., Trisolino, P., Turnbull, J., Van Den Bulk, P., Van Dinther, D., Vermeulen, A., Viner, B., Vitkova, G., Walker, S., Watson, A., Wofsy, S. C., Worsey, J., Worthy, D., Dickon, Y., Zaehle, S., Zahn, A., and Miroslaw, Z.: CarbonTracker CT2022, 10.25925/Z1GJ-3254, 2023.
Meirink, J. F., Bergamaschi, P., and Krol, M. C.: Four-dimensional variational data assimilation for inverse modelling of atmospheric methane emissions: method and comparison with synthesis inversion, Atmos. Chem. Phys., 8, 6341-6353, 10.5194/acp-8-6341-2008, 2008.
Miller, J. B., Lehman, S. J., Andrews, A., Sweeney, C., McKain, K., Tans, P., Southon, J., Hammer, S., Turnbull, J., and Xu, X.: Numerical Representation of Contemporary Atmospheric Δ14CO2: 2. Three-Dimensional Simulation and Comparison With Observations, Global Biogeochemical Cycles, 39, 10.1029/2025gb008523, 2025.
Turnbull, J. C., Sweeney, C., Karion, A., Newberger, T., Lehman, S. J., Tans, P. P., Davis, K. J., Lauvaux, T., Miles, N. L., Richardson, S. J., Cambaliza, M. O., Shepson, P. B., Gurney, K., Patarasuk, R., and Razlivanov, I.: Toward quantification and source sector identification of fossil fuel CO2 emissions from an urban area: Results from the INFLUX experiment, Journal of Geophysical Research: Atmospheres, 120, 292-312, https://doi.org/10.1002/2014JD022555, 2015.
Turnbull, J. C., Karion, A., Davis, K. J., Lauvaux, T., Miles, N. L., Richardson, S. J., Sweeney, C., McKain, K., Lehman, S. J., Gurney, K. R., Patarasuk, R., Liang, J., Shepson, P. B., Heimburger, A., Harvey, R., and Whetstone, J.: Synthesis of Urban CO2 Emission Estimates from Multiple Methods from the Indianapolis Flux Project (INFLUX), Environmental Science & Technology, 53, 287-295, 10.1021/acs.est.8b05552, 2019.